International Communications in Heat and Mass Transfer 84 (2017) 35–40

Contents lists available at ScienceDirect

International Communications in Heat and Mass Transfer

journal homepage: www.elsevier.com/locate/ichmt

Development of heat and mass transfer model for condensation

Qie Shen, Daming Sun *, Shiyue Su, Ning Zhang, Tao Jin

College of Energy Engineering, Zhejiang University, Hangzhou 310027, PR China

ARTICLE INFO

Available online xxxx

Keywords:
Condensation model
Interfacial temperature
Condensation frequency
Phase interface
Numerical simulation

ABSTRACT

Divergence and the interfacial temperature deviation are the two main problems in condensation simulation with the Lee model. Based on the heat transfer analysis at the vapor-liquid interface, a correlation is revealed describing the relationship between interfacial temperature deviation and the model parameters, $q_i \approx (T_{sat} - T_i)(Ak_v)^{0.5}$ where $A = h_{fg} r\rho_v / T_{sat}$. With this correlation, the determination of the condensation frequency r is no longer empirical. Furthermore, the correlation indicates that the thermal conductivity of vapor plays an important role. Accordingly, an improved model is proposed amplifying the thermal conductivity of vapor in the phase interaction region. The model is verified with the Nusselt problem and the impacts of the model parameters are discussed and compared with the original Lee model. It is shown that the interfacial temperature deviation is reduced by the amplified thermal conductivity of vapor. The convergence is maintained by increasing both A and k_v synchronously. Verification is also obtained on the forced convection condensation of R134a. The correlation predicts a temperature deviation at 0.1 K and the numerical result successfully reaches 0.12 K.

1. Introduction

The vapor-liquid phase change process is highly concerned in both academia and industry. It is essential in heat exchangers such as evaporators, boilers and condensers. The VOF method [1] is well accepted in modeling multiphase flow, in which the vapor-liquid interface can be tracked via the conservation of volume fraction. The Lee model [2] is widely applied in modeling evaporation-condensation phenomena. The model defines the phase interaction term according to the temperature deviation from the saturated temperature. With the help of the Lee model, the heat exchanger design, especially for the refrigerants, has made a significant progress in predicting the performance of coil tubes [3], flattened tubes [4], mini-tubes [5–7], mini/micro-channels [8,9] etc.

The Lee model originates from the molecular kinetic theory. When the Hertz-Knudsen equation works together with the Clausius Clapeyron equation [10], the mass flux and the heat flux across the vapor-liquid interface can be yielded as

$$\dot{m}_i = \frac{2\kappa}{2-\kappa} h_{fg} \sqrt{\frac{1}{2\pi R T_{sat}}} \frac{\rho_v \rho_l}{\rho_l - \rho_v} \frac{T_{sat} - T}{T_{sat}} \tag{1}$$

$$\dot{q}_i = \dot{m}_i h_{fg} = \frac{2\kappa}{2-\kappa} h_{fg}^2 \sqrt{\frac{1}{2\pi R T_{sat}}} \frac{\rho_v \rho_l}{\rho_l - \rho_v} \frac{T_{sat} - T}{T_{sat}}. \tag{2}$$

R is the specific gas constant, J/kg-K; κ is the condensation coefficient defined as the ratio of the molecules absorbed by liquid to the total molecules impinged from vapor to liquid, $0 < \kappa \le 1$.

Considering the application in VOF method, usually there is no real interfacial surface but an interfacial layer (where $0 < \alpha_v < 1$) as thick as several cells. Introducing an assumption that the subcooled vapor contains a number of nucleated liquid drops of which the surface-to-volume ratio is R_{sv}, the mass transfer rate of the interfacial cell becomes

$$\dot{m}_l = \alpha_v R_{sv} \dot{m}_i = \alpha_v R_{sv} \frac{2\kappa}{2-\kappa} h_{fg} \sqrt{\frac{1}{2\pi R T_{sat}}} \frac{\rho_l \rho_v}{\rho_l - \rho_v} \left(\frac{T_{sat} - T}{T_{sat}} \right). \tag{3}$$

Introducing a parameter r defined as

$$r = R_{sv} \frac{2\kappa}{2-\kappa} h_{fg} \sqrt{\frac{1}{2\pi R T_{sat}}} \frac{\rho_l}{\rho_l - \rho_v}. \tag{4}$$

* Corresponding author.
E-mail address: sundaming@zju.edu.cn (D. Sun).

http://dx.doi.org/10.1016/j.icheatmasstransfer.2017.03.009
0735-1933/

Nomenclature

A	coefficient defined in Eq. (9)
A_i	interfacial area, m^2
B	coefficient defined in Eq. (13)
F	volumetric surface tension force, N/m^3
$\vec{g}$	gravity, m/s^2
H	enthalpy, J/kg
h_{fg}	latent heat, J/kg
K	interface curvature, m^{-1}
k	thermal conductivity, W/m-K
k'	amplified vapor thermal conductivity, W/m-K
L	thickness of thermal interface layer, m
$\dot{m}_i$	mass flux through phase interface, kg/m^2-s
$\dot{m}_l$	volumetric mass transfer rate from vapor to liquid, kg/m^3-s
$\dot{m}_v$	volumetric mass transfer rate from liquid to vapor, kg/m^3-s
n	amplify factor of thermal conductivity
p	pressure, Pa
$\dot{q}$	volumetric energy source, W/m^3
$\dot{q}_i^*$	non-dimensional interfacial energy source
$\dot{q}_i$	interfacial energy source, W/m^2
R	specific gas constant, J/kg-K
R_{sv}	surface-to-volume ratio, m^{-1}
r	condensation frequency, s^{-1}
T	temperature, K
T^*	non-dimensional temperature
$\vec{u}$	velocity vector, m/s
x, y	Cartesian coordinate, m
x^*	non-dimensional Cartesian coordinate

Greek symbols

α	volume fraction
β	the A/k' value of CASE I
γ	the Ak' value of CASE I
κ	condensation coefficient, the ratio of absorbed molecules at phase interface
μ	viscosity, kg/m-s
ρ	density, kg/m^3
σ	surface tension, N/m

Subscripts

eff	effective
i	interfacial
l	liquid
sat	saturated
T	turbulence
v	vapor

Eq. (3) can be simplified and the Lee model for condensation is yielded as

$$\dot{m}_l = -\dot{m}_v = r\alpha_v\rho_v\frac{T_{sat}-T}{T_{sat}},\quad \text{if } T<T_{sat}. \tag{5}$$

Correspondingly, for evaporation

$$\dot{m}_v = -\dot{m}_l = r\alpha_l\rho_l\frac{T-T_{sat}}{T_{sat}},\quad \text{if } T>T_{sat}. \tag{6}$$

Therefore, the energy source term becomes

$$\dot{q} = \dot{m}_l h_{fg} = -\dot{m}_v h_{fg}. \tag{7}$$

Here r is called the evaporation/condensation frequency, with a unit of s^{-1}. The frequency is regarded as the key parameter in the Lee model, and is usually determined empirically. The experience showed that the proper r varies in different problems and even alters for different cases in the same problem. What's more, taking a brief scan on the literatures, it is learnt that the proper r in evaporation can be as low as 0.1 s^{-1} [11] while in condensation can be as high as 10^6 s^{-1} [9]. From Eqs. (5) and (6), it is clear that the larger the temperature difference is, the larger the mass source term is. In other words, when r is fixed, the intensity of the phase change highly depends on the temperature difference. A simplified interfacial energy source is adopted by researchers, i.e.

$$\dot{q} = A(T_{sat}-T). \tag{8}$$

Zhang et al. [12] set the coefficient A at 10^{20} when modeling capillary blocking in miniature tube condensation. Yuan et al. [13] investigated the condensation in plate-fin heat exchanger, setting $A = 10^{10}$. Eq. (8) can be considered as a simplified Lee model neglecting the contribution of volume fraction α. The fluid density and saturated temperature are both constant, then adjusting the multiplier A is equivalent to adjusting r.

Over the decades, the determination of coefficient r is highly empirical. Seen from Eq. (4), despite the physical properties there are two parameters left unknown, R_{sv} and κ. R_{sv} is difficult to measure and κ is even confusing. There are predecessors who tried to measure the condensation coefficient κ, but the yielded data for water ranges from 10^{-3} to 1, across three scales [14]. What's more, usually it is believed that the κ for condensation should be equal to the one for evaporation, but it is confirmed for water and R11 that the condensation one is almost 20% larger than that of evaporation [15, 16]. As a result, the determination of r via physics mechanism remains dim.

Rose reviewed the literatures on the condensation frequency and concluded that it is generally thought that the condensation coefficient is close to unity and the interface temperature drop is negligible for many cases except for liquid metals [17]. Taking κ as 1, Tanasawa calculated the water condensation at a temperature difference of 10 K, and the interfacial heat transfer coefficient is as large as 15.7 MW/m^2-K with an interfacial temperature drop of 0.007 K [10]. It means that the actual interfacial layer should be extremely thin so that it is not practical to apply such a small mesh size in VOF modeling. Therefore, the goal to determine r is rewritten as to find an r large enough to reduce the numerical yielded interfacial temperature drop to an acceptable level.

However, when modeling condensation, complains were frequently heard that only the high value of condensation frequency could sustain the vapor-liquid interface close to the saturated temperature. The problem is that the higher value, the higher risk to diverge. In this paper, a modification on the vapor thermal conductivity in two-phase region is proposed based on model analysis. The contribution of each parameter is discussed and a correlation is proposed to predict the interfacial temperature deviation. The improved model is proved better in both accuracy and convergence.

2. Interfacial heat transfer correlation

Upon the vapor-liquid interface, the energy equation can be reduced to a one dimensional thermal conduction problem by assuming that

① the time variation and the convection term are negligible compared with the latent heat;
② α_v stays 1 before arriving the interface.

The energy equation can be written as

$$k_v \frac{d^2T}{dx^2} - A(T - T_{sat}) = 0, \text{where} A = h_{fg} r \rho_v / T_{sat}. \quad (9)$$

The boundary conditions are

$$x = 0, T = T_{sat}; x = L, T = T_i. \quad (10)$$

The schematic diagram for this problem is shown in Fig. 1. To take a non-dimensional operation, it is introduced that

$$T^* = \frac{T - T_{sat}}{T_i - T_{sat}}, \quad x^* = \frac{x}{L}. \quad (11)$$

Then Eq. (9) becomes

$$\frac{d^2T^*}{dx^{*2}} - B^2 T^* = 0, \text{with} T^*(0) = 0, T^*(1) = 1 \quad (12)$$

$$\text{where} B = \sqrt{\frac{AL^2}{k_v}}. \quad (13)$$

The solution to this problem is

$$T^*(x^*) = \frac{e^{B - Bx^*}\left(e^{2Bx^*} - 1\right)}{e^{2B} - 1}. \quad (14)$$

The curves for T^* according to various B is drawn in Fig. 1. As B turns larger, the curve becomes steeper. Because of the temperature-linear source, most of the changes in T^* will occur at the position adjacent to $x^* = 1$. Correspondingly, most of the phase interaction occurs near the interface. On the other hand, the sharp curve is not possible to describe accurately by a limited number of grids, thus the large B will lead to the convergence problem.

To analyze further, the overall non-dimensional source can be integrated as

$$\dot{q}_i^* = \int_0^1 -B^2 T^*(x^*) dx^* = -\frac{B(e^B - 1)}{e^B + 1}. \quad (15)$$

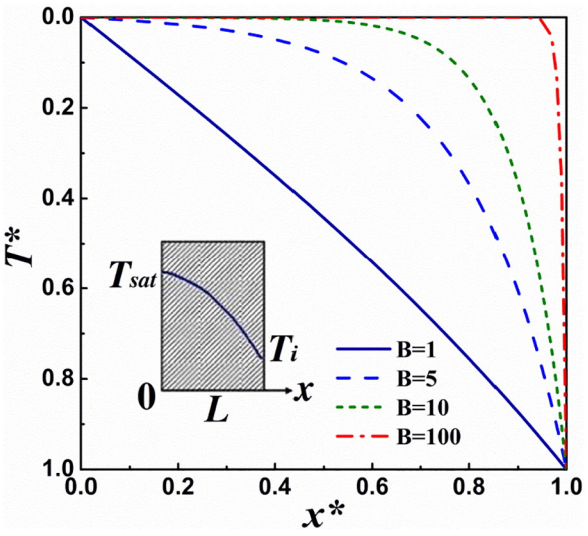

Fig. 1. The 1D conduction problem with internal source.

Then the actual heat source can be yielded when dimensional parameters substitute back.

$$\dot{q}_i = \int_0^L -A(T - T_{sat}) dx = \sqrt{Ak_v}(T_{sat} - T_i)\frac{e^B - 1}{e^B + 1} \quad (16)$$

For $B > 3.66$, there is $0.95 < \frac{e^B - 1}{e^B + 1} < 1$. Because of the large scale of A, this condition is easy to reach. Then the actual heat source becomes

$$\dot{q}_i \approx (T_{sat} - T_i)\sqrt{Ak_v}. \quad (17)$$

The correlation tells that for a given heat flux, the rise of A and k_v could help to minimize the interfacial temperature deviation. However, the rise of A (equivalent to the rise of r) comes up with the risk of divergence. To alter the k_v within the two phase region is a promising approach. As the definition of B shows, taking L as a constant, if A/k_v stays the same, B stays the same. The same B will result in the same T^* curve. Therefore, if the two parameters A and k_v are amplified at the same rate, the T^* curve will not be sharper. In other words, it decreases the interface temperature deviation while maintain the convergence.

3. Improved condensation model

According to Eq. (17), an improved condensation model is proposed. The equations of the Lee model are inherited, i.e. Eq. (5) is applied to describe the mass transfer from vapor to liquid, and Eq. (7) is for the latent heat extraction.

In the VOF method, the material properties are volume-fraction-averaged:

$$\rho = \alpha_v \rho_v + \alpha_l \rho_l \quad (18)$$

$$\mu = \alpha_v \mu_v + \alpha_l \mu_l \quad (19)$$

$$k = \alpha_v k_v + \alpha_l k_l. \quad (20)$$

However, in the present model, the conductivity is amplified within the subcooled two-phase region, expressed as:

$$k = \alpha_v k' + \alpha_l k_l, \text{ if } T < T_{sat} \quad (21)$$

where $k' = nk_v$. For classic model, $n = 1$, Eq. (21) reduces to Eq. (20). In the present model, n is set to 10 or 100 to enhance the energy transportation within the two-phase region.

The proposed model is applied to solve the Nusselt condensation of water and the forced convection condensation of refrigerant R134a. Both problems are considered as steady, while the former one is laminar flow and the latter one turbulent flow.

The governing equations are written as follows.

The volume fraction equation:

$$\alpha_v + \alpha_l = 1. \quad (22)$$

The continuity equations:

$$\nabla \cdot \left(\rho \vec{u}\right) = 0. \quad (23)$$

The momentum equations:

$$\text{For laminar flow}: \quad \nabla \cdot \left(\rho \vec{u}\,\vec{u}\right) = -\nabla p + \nabla \cdot \left(\mu \nabla \vec{u}\right) + \rho \vec{g} + F. \quad (24)$$

$$\text{For turbulent flow}: \quad \nabla \cdot \left(\rho \vec{u}\,\vec{u}\right) = -\nabla p + \nabla \cdot \left[(\mu + \mu_T)\left(\nabla \vec{u} + \nabla \vec{u}^T\right)\right] + \rho \vec{g} + F. \quad (25)$$

The surface tension force F is considered using the continuum surface force (CSF) model [18], expressed as

$$F = \sigma \frac{\alpha_v \rho_v K_v \nabla \alpha_v + \alpha_l \rho_l K_l \nabla \alpha_l}{0.5(\rho_v + \rho_l)} \tag{26}$$

where σ is the surface tension; K is the surface curvature obtained from

$$K_l = -K_v = -\nabla \cdot \left(\frac{\nabla \alpha_l}{|\nabla \alpha_l|} \right). \tag{27}$$

The energy equation:

$$\text{For laminar flow}: \quad \nabla \cdot \left(\rho \vec{u} H \right) = \nabla \cdot (k \nabla T) + \dot{q}. \tag{28}$$

$$\text{For turbulence flow}: \quad \nabla \cdot \left(\rho \vec{u} H \right) = \nabla \cdot (k_{eff} \nabla T) + \dot{q}. \tag{29}$$

Here, the total enthalpy H is mass-weighted-averaged

$$H = \frac{\alpha_v \rho_v H_v + \alpha_l \rho_l H_l}{\alpha_v \rho_v + \alpha_l \rho_l}. \tag{30}$$

The turbulent effective thermal conductivity is calculated as

$$k_{eff} = k + \frac{c_p \mu_T}{0.85}. \tag{31}$$

The SST model [19] is selected to solve the turbulence parameters as Ref [20] suggested.

The numerical scheme of PISO is adopted for pressure-velocity coupling. The discretization scheme for pressure is PRESTO, while QUICK is chosen for both momentum and energy equations. For the volume fraction, the Compressive scheme is selected.

4. Problems for verification

4.1. Nusselt condensation problem

The Nusselt condensation problem describes the vapor condensation along a vertical subcooled wall. The interface temperature is considered at the saturated temperature, and the down flow condensate film is driven by gravity.

Various values of condensation frequency are applied as listed in Table 1. Taking CASE I as a standard case, the A/k' value of which is defined as β while Ak' defined as γ. The CASE IV and V increase the two parameters at the same rate and keep the value A/k' as β. On the other hand, CASE IV has an Ak' of 100γ, equivalent to CASE III. For CASE V, it takes $10{,}000\gamma$, the highest of all the cases.

The computation region is 2D, with a size of $x \times y = 10$ mm $\times$ 100 mm. The mesh number is $x \times y = 100 \times 130$. The smallest cell is 1 μm × 1 μm, while the interval size grows gradually as shown in Fig. 2. The gravity direction is along x axis. The blue boundary is a cold wall at 363.15 K, while the other boundaries are set as pressure outlets at 1 atm. The pressure outlet properties are specified as follows: If there is backflow, the backflow is fresh vapor at 373.15 K; the backflow direction is determined by the neighbor cell.

Table 1
Case settings.

	r	k'	A/k'	Ak'
CASE I	10,000 s^{-1}	k_v	β	γ
CASE II	100,000 s^{-1}	k_v	10β	10γ
CASE III	1,000,000 s^{-1}	k_v	100β	100γ
CASE IV	100,000 s^{-1}	$10k_v$	β	100γ
CASE V	1,000,000 s^{-1}	$100k_v$	β	$10{,}000\gamma$

4.2. Forced convection condensation problem

The gravity effect on the condensation of R134a inside a vertical miniature tube was investigated by Da Riva and Del Col [20]. The tube is 1 mm in diameter and 125 mm in length. The tube is 10 K subcooled. At a mass flux of 100 kg/m^2 s, the condensation frequency r was set to 7.5×10^5 s^{-1}, and the yielded interfacial temperature was 311.95 K (38.8 °C), 1.2 K below the saturation temperature 313.15 K (40 °C). A 2D axisymmetric model is built with a similar mesh distribution to Fig. 1. The grid number is 80 along the radius and 125 along the tube length. The smallest cell is 0.5 μm × 0.5 μm. Adopting the proposed model, the condensation frequency is set to 1,000,000 s^{-1}, while the conductivity is amplified 100 times.

5. Results and discussion

5.1. Nusselt condensation

The film thicknesses are shown in Fig. 3. The average interfacial temperature is given in the figure. From CASE I to III, it is concluded that a higher condensation frequency gives an average interfacial temperature closer to saturated temperature while the film thickness approaches the Nusselt thickness. It is expected that setting $r = 10{,}000{,}000$ s^{-1} will achieve an even better result. However, the CASE III with $r = 1{,}000{,}000$ s^{-1} becomes difficult to converge. For comparison, when modeling condensation of R134a, Da Riva and Del Col [21] tried a largest value of $r = 750{,}000$ s^{-1}, but still the deviation from saturated temperature is over 1 K. The convergence problem is an obstacle between the ideal result and the Lee model. Among all the cases, the performances are almost the reflection of the value Ak'. Because of the same Ak', the film thicknesses of CASE III and IV are similar and their average interfacial temperatures are close. CASE V achieves a great accuracy and the interface temperature deviation is only 1.1 K on average.

To help understand the performance of the Lee model, the temperature distribution at the bottom edge of the computation domain is displayed in Fig. 4, together with the VOF value and the condensation mass flux. With the micrometer scale meshes, the figure is able to shown the three sections of the temperature curves. The first section belongs to the liquid film, where the temperature distribution is almost linear. The second section is a gradual transition from the interfacial

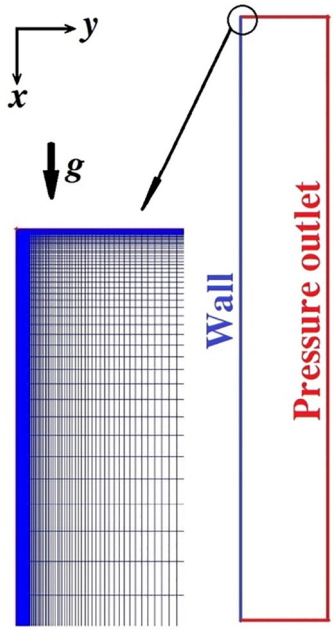

Fig. 2. The computation domain and the near wall mesh.

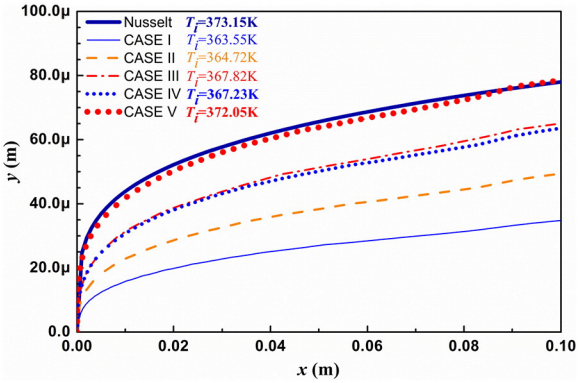

Fig. 3. The film thickness of various cases.

temperature to the saturated temperature. The third one is the uniform saturated temperature in the pure vapor region.

The second section is the one to be especially concerned. It can be regarded as the thermal interface which is encompassed by temperature between the saturated vapor and the liquid film surface, distinguished from the phase interface defined by volume fraction. The temperature in the second section is lower than the saturated temperature, thus all the cells in this section has a condensation mass transfer rate. As plotted in Fig. 4, arising from the pure vapor section, the mass transfer rate grows quite slow until approaching the liquid film surface where the major boost occurs. The area covered by the mass transfer rate curve is the cross-sectional mass flux from vapor to liquid. It can be learnt that the intensity of phase interaction rises with r, as well as the film thickness.

The setting of CASE IV is unique. First, it has an A/k' value equivalent to CASE I, thus in the thermal interface, the temperature curves of these two cases are similar. Second, it has the same r to CASE II, but because of the amplified k, the slope of mass transfer rate curve at the vapor side is gentler. Third, the Ak' values of CASE IV and III are the same, so that the performances of the two cases are close, as shown in Fig. 3. However, the temperature curve of CASE III is sharper while CASE IV smoother. It is also presented in the mass transfer rate curves that there is a pulse for CASE III but a much smoother curve for CASE IV. It means that CASE IV achieves both a similar performance and a better convergence.

CASE V shows the best performance. With the help of the largest Ak' value, the temperature curve is the closest to the ideal Nusselt line. The temperature curve in the thermal interface is a gradual slope, which makes the pulsing of mass transfer rate curve well-controlled. Due to the well distributed mass transfer rate, the highly improved performance is no longer followed by the convergence problem.

The temperature curves in Fig. 4 also provide another way to understand the impact of k_v. Because of the energy conservation at the liquid film surface, the temperature gradient follows

$$k_l \frac{dT_l}{dy} = k_v \frac{dT_v}{dy} \quad \Rightarrow \quad \frac{dT_l}{dy} / \frac{dT_v}{dy} = k_v / k_l. \tag{32}$$

The formula tells that the change of gradient of temperature at the interface follows the ratio of thermal conductivity. Since the vapor conductivity is lower than that of liquid, the temperature gradient of liquid will always be smaller than that of vapor, as shown by the left part of Fig. 4. The larger gradient of temperature at the vapor side will result in a larger temperature drop across the thermal interface. After the amplification of vapor conductivity, the interfacial temperature deviation is reduced with the vapor side temperature gradient reduced, as shown by the right part of Fig. 4. This is an important reason for the large interface temperature deviation by the original Lee model. What is more, it also explains why in boiling or evaporation the Lee model can work with a low r and convergence problem is seldom reported. Taking the sharp interface method [22], Sun et al. applied a source term at the interfacial cell and successfully modeled pool boiling by setting liquid conductivity to zero [23], and further proposed a method that to set the conductivity of both phases at the same value [24], which is equivalent to an operation to increase the ratio k_v/k_l. The present model explains why these operations could help and how to do better.

Additionally, it is found that the amplified k_v also widens the thermal interface when comparing CASE III vs. V, or CASE II vs. IV. Since the amplified A will narrows the thermal interface while increase the risk of divergence, it is an interesting property that the conductivity acts in a reverse way. However, both of them help to reduce the interfacial temperature deviation.

Finally, the proposed Eq. (17) can help to determine the proper configuration of r and k'. The prediction of interfacial temperature by the

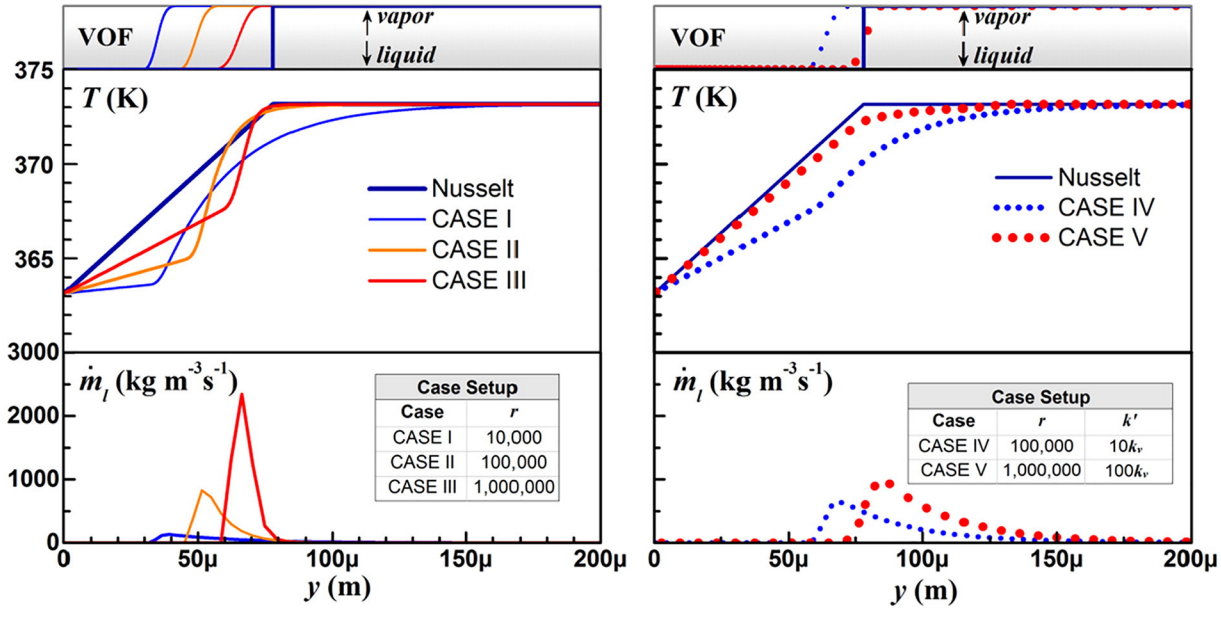

Fig. 4. The temperature distribution, volume fraction and mass flux at $x = 0.1$ m.

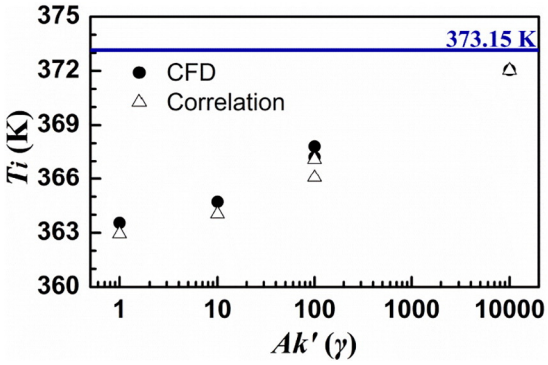

Fig. 5. Interfacial temperature prediction.

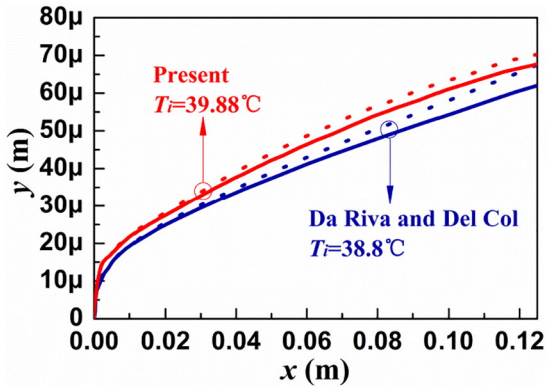

Fig. 6. The R134a forced convection condensation film prediction (solid line: with gravity; dash line: without gravity).

equation is shown in Fig. 5. The CFD yielded interfacial temperature is plotted as solid circles, while the equation prediction from the CFD heat flux is plotted as empty triangles. The results show that the equation can predict the interfacial temperature within an acceptable error. Since the condensation frequency alters in scale level, the performance of Eq. (17) is sufficiently fine.

5.2. Forced convection condensation

In this case, since the reported heat flux is around 20,000 W/m^2, the predicted interfacial temperature deviation by Eq. (17) can achieve 0.1 K. The obtained R134a condensate film is compared with that of Ref. [20] in Fig. 6. It is shown that the condensate film of the present model is a bit thicker than that of the literature. The thicker film is a result of the higher interfacial temperature with the yielded deviation of only 0.12 K from the saturated temperature. Overall, the equation prediction is successful and the improved model works well.

6. Conclusions

The interfacial heat transfer is analyzed for condensation simulation by the Lee model. A relationship between the interfacial temperature deviation and model parameters is built, i.e. $\dot{q}_i \approx (T_{sat}-T_i)\sqrt{Ak_v}$. According to the correlation, an improved model that increase both A and k_v synchronously is proposed. The interfacial temperature deviation is reduced to 1.1 K and the convergence is kept well in the Nusselt condensation problem of water. The yielded film is very close to the Nusselt solution, as well as the temperature distribution.

Furthermore, the correlation is instructive and effective in determining the proper condensation frequency. If the condensation frequency is too large to converge, the amplification of thermal conductivity can be taken based on the correlation. In the forced convection condensation problem of R134a, the model parameters are predicted to yield an interfacial temperature deviation of 0.1 K, and successfully the result reaches 0.12 K as expected.

Acknowledgements

The research is financially supported by the National Natural Science Foundation of China (No. 51406218, No. 51676168).

References

[1] C.W. Hirt, B.D. Nichols, Volume of fluid (VOF) method for the dynamics of free boundaries, J. Comput. Phys. 39 (1) (1981) 201–225.
[2] W.H. Lee, A pressure iteration scheme for two-phase flow modeling, Multiphase Transport Fundamentals, Reactor Safety, Applications, 1, 1980, pp. 407–431.
[3] Z. Yang, X.F. Peng, P. Ye, Numerical and experimental investigation of two phase flow during boiling in a coiled tube, Int. J. Heat Mass Transf. 51 (5–6) (2008) 1003–1016.
[4] J. Zhang, W. Li, S.A. Sherif, A numerical study of condensation heat transfer and pressure drop in horizontal round and flattened minichannels, Int. J. Therm. Sci. 106 (2016) 80–93.
[5] J. Zhang, W. Li, Numerical study on heat transfer and pressure drop characteristics of R410A condensation in horizontal circular mini/micro tubes, Can. J. Chem. Eng. 94 (2016) 1809–1819.
[6] J. Zhang, W. Li, W.J. Minkowycz, Numerical simulation of condensation for R410A at varying saturation temperatures in mini/micro tubes, Numer. Heat Transf. A Appl. 69 (5) (2016) 1–16.
[7] D. Del Col, E. Da Riva, S.V. Garimella, A. Cavallini, The importance of turbulence during condensation in a horizontal circular minichannel, Int. J. Heat Mass Transf. 55 (s 13–14) (2012) 3470–3481.
[8] S. Chen, Z. Yang, Y. Duan, Y. Chen, D. Wu, Simulation of condensation flow in a rectangular microchannel, Chem. Eng. Process. Process Intensif. 76 (2014) 60–69.
[9] S. Bortolin, E. Da Riva, D. Del Col, Condensation in a square minichannel: application of the VOF method, Heat Transf. Eng. 35 (2) (2014) 193–203.
[10] I. Tanasawa, Advances in condensation heat transfer, Adv. Heat Tran. 21 (1991) 55–139.
[11] A. Alizadehdakhel, M. Rahimi, A.A. Alsairafi, CFD modeling of flow and heat transfer in a thermosyphon, Int. Commun. Heat Mass Transf. 37 (3) (2010) 312–318.
[12] Y. Zhang, A. Faghri, M.B. Shafii, Capillary blocking in forced convective condensation in horizontal miniature channels, J. Heat Transf. 123 (3) (2001) 501–511.
[13] J. Yuan, C. Wilhelmsson, B. Sundén, Analysis of water condensation and two-phase flow in a channel relevant for plate heat exchangers, Advanced Computational Methods in Heat Transfer IX, 53, 2006, pp. 351–360.
[14] R. Marek, J. Straub, Analysis of the evaporation coefficient and the condensation coefficient of water, Int. J. Heat Mass Transf. 44 (1) (2001) 39–53.
[15] G.O. Rubel, J.W. Gentry, Measurement of the kinetics of solution droplets in the presence of adsorbed monolayers: determination of water accommodation coefficients, J. Phys. Chem. 88 (14) (1984) 3142–3148.
[16] J. Straub, J. Winter, G. Picker, H. Merte, A. Kono, Study of vapor bubble growth in a supersaturated liquid, 8th European Symposium on Materials and Fluid Sciences in Microgravity, 1992.
[17] J.W. Rose, Condensation heat transfer fundamentals, Chem. Eng. Res. Des. 76 (2) (1998) 143–152.
[18] J.U. Brackbill, D.B. Kothe, C. Zemach, A continuum method for modeling surface tension, J. Comput. Phys. 100 (2) (1992) 335–354.
[19] F.R. Menter, Two-equation eddy-viscosity turbulence models for engineering applications, AIAA J. 32 (8) (1994) 1598–1605.
[20] E. Da Riva, D. Del Col, Effect of gravity during condensation of R134a in a circular minichannel, Microgravity Sci. Technol. 23 (S1) (2011) 87–97.
[21] E. Da Riva, D. Del Col, Numerical simulation of laminar liquid film condensation in a horizontal circular minichannel, J. Heat Transf. 134 (5) (2012) 807–824.
[22] H. Lee, C.R. Kharangate, N. Mascarenhas, I. Park, I. Mudawar, Experimental and computational investigation of vertical downflow condensation, Int. J. Heat Mass Transf. 85 (2015) 865–879.
[23] D. Sun, J. Xu, L. Wang, Development of a vapor–liquid phase change model for volume-of-fluid method in FLUENT, Int. Commun. Heat Mass Transf. 39 (8) (2012) 1101–1106.
[24] D. Sun, J. Xu, Q. Chen, Modeling of the evaporation and condensation phase-change problems with FLUENT, Numer. Heat Transf. B Fundam. 66 (4) (2014) 326–342.